Isospin splitting of the giant dipole built on the isobaric analog state

S. Mordechai
Ben-Gurion University of the Negev, Beer-Sheva 84105 Israel,
University of Texas at Austin, Austin, Texas 78712,
and University of Pennsylvania, Philadelphia, Pennsylvania 19104

N. Auerbach
Tel Aviv University, Tel Aviv, Israel

H. T. Fortune
University of Pennsylvania, Philadelphia, Pennsylvania 19104

C. L. Morris
Los Alamos National Laboratory, Los Alamos, New Mexico 87545

C. Fred Moore
University of Texas at Austin, Austin, Texas 78712
(Received 17 June 1988)

We report the first observation of the isospin splitting of the giant dipole resonance built on the isobaric analog state. Three giant resonances were observed in (π^+,π^-) double charge exchange (at $T_\pi=292$ MeV) on ^{56}Fe at excitation energies of 25.7, 30.0, and 33.5 MeV ($Q=-31.4$, -35.7, and -39.2 MeV). Angular distributions were measured for the resonances and each observed to have a dipole shape. The cross-section ratios of the resonances are in close agreement with simple isospin geometry arguments for an isovector excitation built on the isobaric analog state. The summed cross section agrees well with simple sequential-model calculations in which the intermediate states arise from single charge exchange to the isobaric analog state and to the giant dipole resonance. We identify the three resonances as the isospin members of the charge-exchange dipole built on the isobaric analog state.

I. INTRODUCTION

An exciting development in nuclear physics in recent years has been the observation of giant dipole excitations built on excited nuclear states. Such excitations were predicted by Brink and Axel[1] in the early sixties, but experimental observations of the phenomena were made possible only in recent years[2]—mainly via γ-ray spectra from heavy-ion fusion[3-6] and proton capture (p,γ) reactions.[7-10] Typical spectra from the above studies show an excess yield of high-energy γ rays in the $E1$ region. This excess yield has been interpreted as dipole photons emitted in competition with neutrons in the early stage of the cooling process of the nuclear complex. These studies show some interesting features of the giant dipole resonances (GDR's) in excited nuclei when compared with the corresponding resonances built on the ground state. The energies of the GDR's in heated nuclei follow the well-known ground-state GDR energies as observed, for example, in photonuclear reactions. The measured strengths of the GDR's in excited nuclei are essentially consistent with one classical dipole sum rule. However, the widths of the dipole in excited nuclei are generally substantially larger than the corresponding widths of the dipole built on the ground state. This broadening is attributed to deformation effects at high excitations and spins.[10,11]

The frequency of the dipole in excited nuclei is intimately related to the size of the nucleus, and, therefore, it provides one of the best probes of the shape of nuclei at high excitations.[11] The general features of the GDR in excited nuclei are summarized in a recent review work by Snover.[10] The main difficulties in the interpretation of the γ-ray spectra in the above studies arise from the large widths of both the resonance states and final states and from the large density of states at high excitation energy. Therefore, it is generally difficult to observe a resolved GDR built on discrete excited states, unless a more complicated coincidence experiment between the high-energy γ rays and the excited states is measured.[12,13]

Mesons have proved extremely useful in the study of charge-exchange excitations. Systematic studies of (π^-,π^0) and (π^+,π^0) charge-exchange reactions[14-17] show that the isospin quantum number of the pion and the pion-nucleon $\Delta_{3,3}$ resonance provide a unique tool to study electric isovector resonances such as the dipole, monopole, and quadrupole. The results indicate that isovector GDR's and isobaric analog states (IAS's) are the two most prominent features in the spectra. They have both been observed in (π^+,π^0) [and the GDR also in

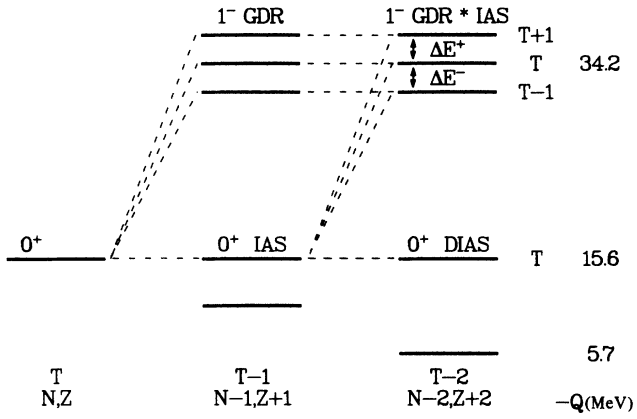

FIG. 1. Schematic energy-level diagram of analog and dipole states observed in single- and double-charge exchange. The listed Q values refer to the case of DCX on ^{56}Fe.

(π^-,π^0)] with typical maximum cross sections of 0.5→1.0 mb/sr. Of course, the IAS is absent in all (π^-,π^0) as well as in (π^+,π^0) on $T=0$ targets. In both these latter cases, the isovector GDR is the only prominent feature of the spectra. Pion double charge exchange (DCX) is thought to proceed predominantly by a two-step (π^+,π^0), (π^0,π^-) mechanism, and therefore should be a unique probe for exciting double giant resonances in nuclei. The lowest in energy of these double resonances is the well-known double isobaric analog state (DIAS) which can be viewed in this context as the simplest double resonance state.

In a recent letter[18] we reported the first observation of giant dipole resonances built on isobaric analog states (GDR⊗IAS) via pion DCX. In a mathematical notation these resonances can be written in terms of charge-exchange dipole and isospin-lowering operators acting sequentially on the ground-state wave function.[18] In the present work we report on the isospin splitting of these new modes of excitations in the case of DCX on ^{56}Fe, and we give a detailed description of the theoretical analysis. Figure 1 shows a schematic energy-level diagram of analog, dipole, and the GDR⊗IAS observed in single and double charge exchange. The three isospin components of the charge-exchange GDR and the GDR superimposed on the IAS are indicated. The predicted energy splitting and strength ratios of the members are discussed later.

II. EXPERIMENT

The measurement was performed with the energetic pion channel and spectrometer (EPICS) at the Clinton P. Anderson Meson Physics Facility (LAMPF) using the pion DCX setup.[19] The isotopic purity and areal density of the ^{56}Fe target were 91.8% and 1.199 g/cm^2. Measurements were taken at $T_\pi=292$ MeV and scattering angles 5°→30° in 5° steps. Electrons were eliminated using a freon-gas Cherenkov detector in the focal plane. A set of veto scintillators separated by graphite wedges in the focal plane was used to reject muons.[20] The system was fine-tuned by placing aluminum absorbers of variable thickness in front of the first scintillator to ensure that no pions reached the veto scintillator. The remaining background was pions resulting from continuum DCX on the target. The choice to run with the highest beam energy available at EPICS ($T_\pi=292$ MeV) results in a lower background level from the continuum DCX spectra since the excitation energy region of interest is away from the inclusive DCX peak. In addition, at this beam energy a large outgoing energy range ($\simeq 50$ MeV) is covered by the acceptance of the spectrometer in a single setting. The variation of the spectrometer acceptance across the focal plane was measured by pion scattering from ^{12}C.

III. RESULTS AND ANALYSIS

A. Discussion of the data

Figure 2 shows the summed ^{56}Fe missing-mass spectrum. In addition to the DIAS transition at $E_x=9.9$ MeV ($Q=-15.6$ MeV) the spectrum shows the existence of three wide peaks labeled GR1, GR2, and GR3 very high in the continuum region at about 15.8, 20.1, and 23.6 MeV above the DIAS. The spectra have been

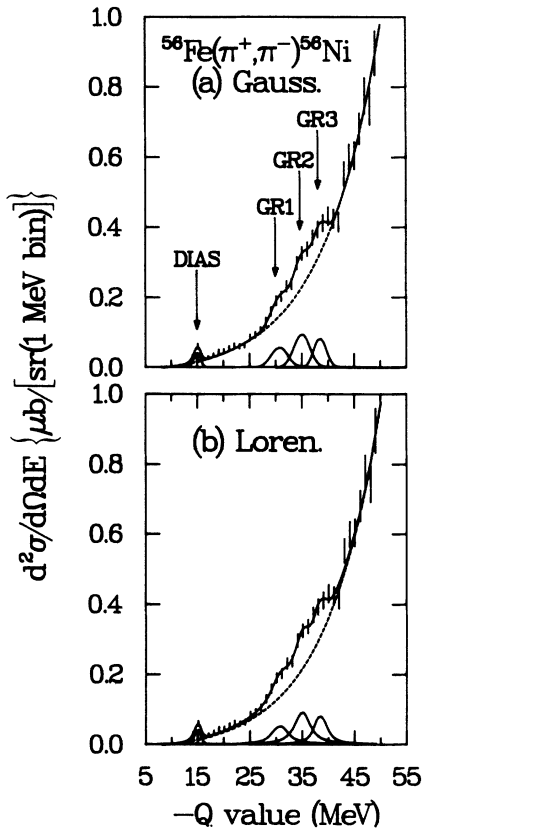

FIG. 2. Summed (angle 5°–30° in 5° steps) cross-section spectrum for (π^+,π^-) reaction on a ^{nat}Fe target at $T_\pi=292$ MeV. (a) Gaussian fit, (b) Lorentzian fit. The arrows indicate the fitted location of the DIAS and the giant resonances. Short vertical lines represent the statistical uncertainty of the data. The dashed line is the fitted background with an exponential shape and the solid line is the fit to the spectrum using NEWFIT.

TABLE I. Parameters of the exponential background[a] obtained from fitting the $^{56}Fe(\pi^+,\pi^-)$ ^{56}Ni spectra for different number of peaks assumed in the fit.

No. of peaks	Γ (MeV)	χ^2 [b]	$R1$	$R2$	$R3$ (MeV)	Ratios $R1$	$R2$	$R3$
1	10	1.38	−0.0208	0.0147	10.78	1	1	1
1	6	1.85	−0.0245	0.0173	11.14	1.18	1.18	1.033
	3.5							
3	3.5	1.19	−0.0225	0.0159	10.96	1.08	1.08	1.017
	2.5							
0		4.74	−0.0307	0.0217	11.93	1.47	1.47	1.11

[a]Background $(E)=R(1)+R(2)\times\exp(E/R3)$.
[b]Reduced χ^2 for entire histogram.

corrected for the measured variation of the spectrometer acceptance as a function of momentum. In an earlier work[18] (where we reported only the gross features of these resonances) we fitted GR1 and GR2 with $\Gamma=6$ MeV (as one peak) and $\Gamma=10$ MeV (fitting all three peaks as one). Based on the angular distribution in ^{56}Fe and the $A^{-1/3}$ dependence of the excitation energy from three targets ^{56}Fe, ^{80}Se, and ^{208}Pb, the resonances were interpreted as a giant dipole built on the isobaric analog state (GDR⊗IAS).[18] In Fig. 2 we fit the spectra with $\Gamma(GR1)=\Gamma(GR2)=3.5$ MeV and $\Gamma(GR3)=2.5$ MeV. These values give the best fit to the data. The spectra can be well fitted using either a Gaussian [Fig. 2(a)] or a Lorentzian [Fig. 2(b)] line shape of variable width for the GR's. For the DIAS only a Gaussian shape was assumed, because its width arises almost entirely from experimental resolution. The background (dashed line) that arises from the DCX cross section to discrete low-lying states and to the continuum was fitted with a three-parameter exponential shape of the form $R1+R2\exp(E/R3)$. The short vertical lines represent the statistical uncertainties of the data. The solid lines are the resulting fits to the spectra. Table I lists the reduced χ^2 and the parameters of the exponential background obtained from fitting the summed spectrum (shown in Fig. 2) with a single peak of width $\Gamma=6$ and 10 MeV, three peaks, and zero peaks (plus the DIAS). The table indicates that the smallest χ^2 is obtained in the case of three peaks. The background shape is affected very little by the above assumptions, except for the unrealistic case of zero peaks. In an attempt to study the influence of the background choice on the result, we fitted the background also using polynomial shapes of the form $R(1)+R(2)\times E+R(3)\times E^2+\cdots$. It was found that comparable fits and cross sections are obtained if third- or higher-order polynomial shapes are used for the background. Figure 3 shows the ^{56}Fe individual spectra at two angles 10° and 15°. The excess yield in the GR region shows up again above background at both angles. In this figure, the three GR's were fitted with a Lorentzian line shape with the same parameters listed earlier.

Figure 4 shows the angular distributions extracted for the sum of the three resonances labeled GR1, GR2, and GR3 in Fig. 2. The cross sections have been extracted with constant $E_x=25.7$, 30.0, and 33.5 MeV at all angles and constrained widths of 3.5 for GR1 and GR2 and 2.5 MeV for GR3. Figure 4(a) shows the cross sections obtained from the Gaussian and Fig. 4(b) from the Lorentzian fit. The two angular distributions are very similar in shape but the Lorentzian fit yields larger cross sections by about 50%. The maximum cross section in both cases is observed at 10° with a slightly smaller cross section at 5°. At scattering angles of 25°–30° the peak is much weaker. The solid and dashed lines in Figs. 4(a) and 4(b) are the results of sequential-model calculations with two different models for the transition density to the isobaric analog state discussed later. Figure 4(c) shows

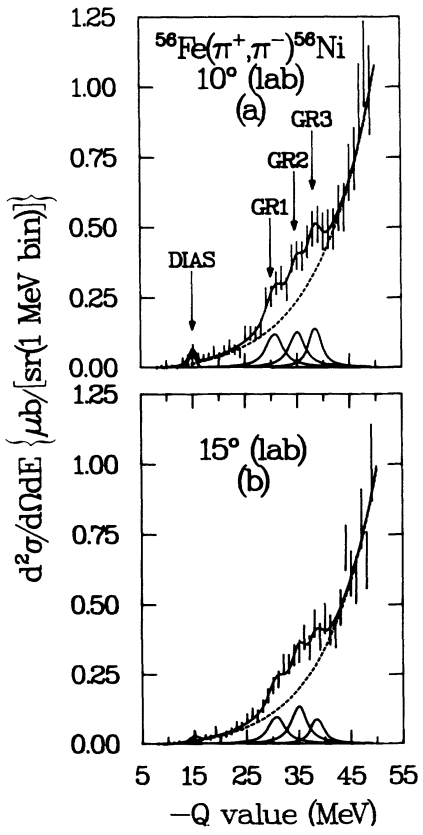

FIG. 3. Double differential cross-section spectrum for (π^+,π^-) reaction on a ^{nat}Fe target at $T_\pi=292$ MeV. (a) $\theta_{lab}=10°$, and (b) $\theta_{lab}=15°$.

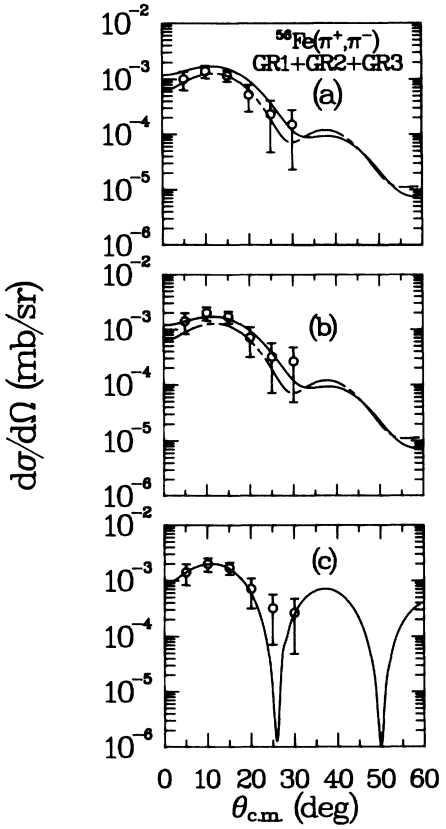

FIG. 4. (a) Angular distribution for the sum of GR1+GR2+GR3 peaks shown in Fig. 2. The cross sections have been extracted using a Gaussian line shape for the giant resonances with a constant width of 3.5 MeV for GR1 and GR2 and 2.5 MeV for GR3 and a constant $E_x=25.7$, 30.0, and 33.5 MeV at all angles. The solid and dashed lines are the results of sequential-model calculations using volume and surface transition densities, respectively, without any normalization factor. (b) Same as (a) but with a Lorentzian fit to the GR's. (c) Data same as (b). The solid line is a Bessel function fit to the data (see text).

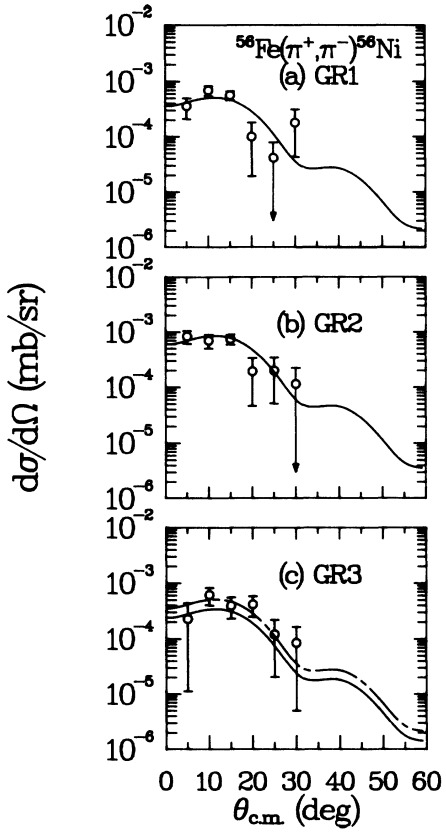

FIG. 5. (a) Angular distribution for the peak labeled GR1 in the DCX spectra on ^{56}Fe shown in Fig. 2. The cross sections have been extracted with a Lorentzian fit using $\Gamma=3.5$ MeV and $E_x=25.7$ MeV. The solid line is the sequential-model calculation (model I) shown in Fig. 4 but normalized by an isospin factor of $\frac{3}{10}$. (b) Same as (a) but for GR2 with $\Gamma=3.5$ MeV and $E_x=30.0$ MeV. The solid line is the CCIA calculation multiplied by a factor of $\frac{5}{10}$. (c) Same as (a) but for GR3 with $\Gamma=2.5$ MeV and $E_x=33.5$ MeV. The solid theoretical curve is normalized by $\frac{2}{10}$, dashed curve by $\frac{3}{10}$.

again the data from the Lorentzian fit. The line in Fig. 4(c) is a $J_1^2(qr)$ fit to the data with a strong absorption radius of 4.1 fm normalized to the 10° data point. This form represents a $\Delta J=1$ angular distribution and is expected for a surface-dominanted diffractive pion scattering process.[21–23]

Figure 5 shows the individual angular distributions of each of the three resonances. The solid lines are the results of a sequential-model calculation (using the volume transition for the IAS) multiplied by the predicted isospin factor discussed later. Each one of the three GR's has significantly a smaller width than the GDR width reported in (π^+,π^0) single-charge-exchange (SCX) data.[24] In the SCX studies the GDR generally includes more than one isospin member because of the limited (6→8 MeV) energy resolution of the π^0 spectrometer. For example in ^{60}Ni ($T=2$ as the present ^{56}Fe) the SCX GDR splits into three components with ratios of 9:5:1.[25] However, experimentally the GDR shows up as a single peak in SCX with $\Gamma=6.4\pm1.7$ MeV.[24] If we use our energy splitting and widths from ^{56}Fe for the ^{60}Ni case and fold the energy resolution of the π^0 spectrometer ($\Gamma_{exp}\simeq7$ MeV), the three peaks indeed produce a single peak (slightly asymmetric) with $\Gamma=7.1$ MeV (after unfolding Γ_{exp}), in close agreement with the above observation. Therefore the present data provide the first observation of isospin splitting of the analog GDR in the same nucleus. Previously, useful information on isospin splitting of the charge exchange GDR was obtained by comparing (π^-,π^0) and (π^+,π^0) yields, since (π^-,π^0) populates only the $(T+1)$ member whereas (π^+,π^0) populates predominantly the $(T-1)$ member.[16,24] The slightly smaller width of GR3 (the $T=3$ component) relative to the lower two components in the present work may be attributable to the fact that a $T=3$ state in ^{56}Ni cannot decay either via proton or via neutron emission to the low-lying states of the neighboring nuclei. In addition, the spreading width is also expected to be smaller for a $T=3$ state in comparison with the lower T members. Therefore it should have a smaller width relative to GR1 ($T=1$) and GR2 ($T=2$).

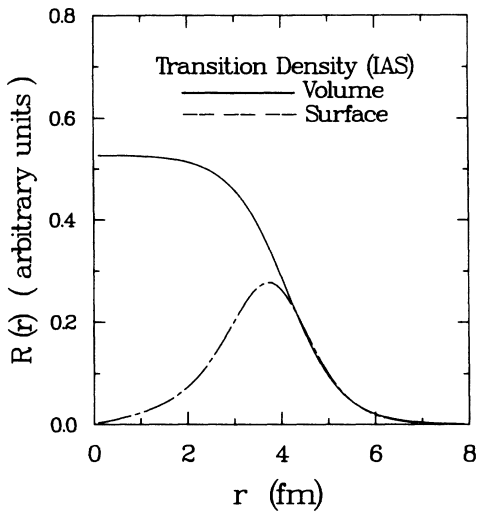

FIG. 6. Volume- (solid) and surface-peaked (chain-dashed) transition densities used for the isobaric analog state in the sequential-model calculations shown in Figs. 4 and 5 (see text).

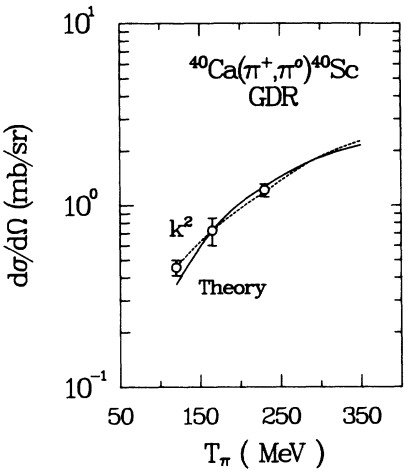

FIG. 7. Experimental cross section for the GDR in $^{40}Ca(\pi^+,\pi^0)$ reaction as a function of pion beam energy compared with k^2 dependence (dashed) and sequential-model calculations (solid) with constant dipole transition strength normalized to the cross section at 165 MeV.

B. Sequential model analysis

A calculation has been performed for the GR's using the pion coupled-channel impulse-approximation code (CCIA) NEWCHOP.[26] The coupled-channel calculations included the ground state, the IAS, the GDR, and the GDR⊗IAS. The collective model has been used to obtain the radial shape of the transition density for the dipole,

$$\rho_{\rm tr}(r) = -(\beta c)\frac{d\rho(r)}{dr} , \tag{1}$$

where $\rho(r)$ is the nuclear ground-state density which was parametrized using a two-parameter Fermi function with half-density radius $c = 4.111$ fm and diffuseness $a = 0.558$ fm as derived from electron scattering.[27] The strength parameter β was adjusted as outlined later. For the transition to the isobaric analog state we used two different transition densities: one volume and one surface peaked. The volume transition density (model I) was assumed for simplicity to have the same radial distribution as the ground-state density, but normalized to the neutron excess in the target nucleus:

$$\rho_{\rm vol}(r) = \frac{N-Z}{A}\rho(r) . \tag{2}$$

The surface transition density (model II), which provides a more realistic shape for the $\rho_{\rm exc}$ density, was taken as a derivative of a two-parameter Fermi ($2pF$) function. Figure 6 shows the two different transition densities used for the isobaric analog state in the sequential-model calculations.

Since there is no pion SCX data available for the GDR at 292 MeV, a calculation was performed at 165 MeV and the strength of the SCX dipole was adjusted to give the experimental peak cross section of 792 μb/sr measured for the GDR on ^{60}Ni at $T_\pi = 165$ MeV.[24] The deduced dipole transition strength at 165 MeV was then used to calculate the dipole cross section at 292 MeV (see Table II). This method was tested by calculating the energy dependence of the SCX cross section for the GDR. Figure 7 shows the SCX data for the GDR on ^{40}Ca at

TABLE II. Results from double-charge-exchange reaction on ^{56}Fe at an incident pion energy $T_\pi = 292$ MeV compared with sequential-model analysis.

			$d\sigma/d\Omega_{\rm max}$ (experiment)		$d\sigma/d\Omega_{\rm max}$ (theory)	
Peak	E_x (MeV)	Γ (MeV)	Gaussian (μb/sr)	Lorentzian (μb/sr)	Model I[a] (μb/sr)	Model II[b] (μb/sr)
DIAS	9.9±0.05	1.3±0.2[c]	0.24±0.05[d]			
GR1	25.7±0.4	3.5±1.1	0.48±0.09	0.69±0.14	0.51	0.38
GR2	30.0±0.4	3.5±0.8	0.51±0.10	0.83±0.19	0.85	0.64
GR3	33.5±0.3	2.5±0.9	0.41±0.14	0.61±0.21	0.34	0.26
Sum			1.40±0.19	2.13±0.32	1.70	1.28

[a]Using volume transition density of the form $[(N-Z)/A]\rho_{\rm g.s.}(r)$ for the IAS, normalized to the measured cross sections in SCX.

[b]Using surface transition density for the IAS (Fig. 6).

[c]Resolution width only, due primarily to target thickness.

[d]DIAS cross section at 5° corrected for the isotopic enrichment of the target (91.8%).

120, 165, and 230 MeV. The data indicate that the GDR cross section increases almost linearly with k^2, where k is the incoming pion momentum (dashed line). The impulse-approximation calculation with a constant dipole transition density, and without any energy shift for the incoming pions[28] (solid) reproduces this energy dependence very well. The k^2 dependence is a consequence of the strong absorption model and is discussed in Ref. 29.

For the IAS transition we normalized the transition strength to give a 0° cross section of 860 μb/sr (at 292 MeV) obtained using the function[30,31]

$$\sigma_{\rm IAS}(0°)=18(N-Z)A^{-1.10}\ \mu{\rm b/sr}\ . \tag{3}$$

The pion distortion is computed using the Kisslinger[32] form for the pion-nucleus potential. The isoscalar and isovector parameters of the elementary t matrix were taken from phase shifts of Rowe, Salomon, and Landau.[33]

C. Comparison with the data

Figure 4(a) shows the results of these calculations without any additional normalization factor. The solid line was obtained using the volume transition density and the dashed line using the surface transition density. The calculated cross sections for the GDR⊗IAS shown in Figs. 4 and 5 are found to peak near $11^\circ_{\rm c.m.}$. This is an expected result for coupling of an analog transition (which peaks at 0°) with a dipole transition (which peaks around 11°). Figure 4(b) shows the same calculations but compared with the cross sections extracted from the Lorentzian fit. The calculations with volume transition density predict a larger cross section for the GDR⊗IAS by about 50% than those obtained using the surface transition density. Both calculations predict the correct shape of the angular distribution for the sum of GR1+GR2+GR3. The dashed line gives a better fit in magnitude in Fig. 4(a), while the solid line reproduces better the cross sections extracted with the Lorentzian fit in Fig. 4(b).

In Fig. 5 we show the data for each of the resonances separately. The curves calculated using the volume transition density have been multiplied by factors of 0.3, 0.5, and 0.2 for GR1, GR2, and GR3, respectively, as required from simple isospin arguments discussed later. Except for GR3, which has an enhanced cross section relative to the prediction, the sequential-model calculations (model I) give an impressive fit to the data. The chain-dashed line in Fig. 5(c) is the result of the same calculations but scaled up arbitrarily by 50%. Therefore the angular distribution measurement on ^{56}Fe and the strength ratios give strong support for the identification of these resonances as the isospin members of the giant dipole built on the isobaric analog state (or equivalently, as isobaric analogs of the charge exchange giant dipoles). Additional support for this identification came from the $A^{-1/3}$ variation of the excitation energy of the GR's above the DIAS and the cross section ratio σ(GR)/σ(DIAS).[18]

D. Discussion

The splitting of the GDR⊗IAS can in general arise from three different sources. *(a) Deformation effects.* In deformed nuclei with axial symmetry, a dipole splits into two components arising from vibrations along the major and minor axis of the nucleus. *(b) Spin coupling.* For nuclei with $J_i \geq 1$, the GDR splits into three members with $J_f=J_i-1$, J_i, and J_i+1. In the simplest case of even-even target nuclei the GDR⊗IAS has a *single J^π value of* 1^-. *(c) Isospin splitting.* For $T\geq 1$ target nuclei, the charge exchange dipole splits into three members with $T-1$, T, and $T+1$. In the present case, $^{56}{\rm Fe}_{\rm gs}$ has only a small deformation and $J_i=0^+$, therefore isospin coupling is the predominant source for the observed energy splitting.

For $T\geq 1$ target nuclei, a charge-exchange GDR built on the IAS will split into three components with isospin $T-1$, T, and $T+1$ arising from coupling of one unit of isospin to a state with isospin T (Fig. 1). Simple isospin geometry arguments predict relative strengths for the GDR⊗IAS members:

$$\sigma(T-1):\sigma(T):\sigma(T+1) = \frac{(2T-1)(T-1)}{T(2T+1)}:\frac{(2T-1)}{T(T+1)}:\frac{3}{(2T+1)(T+1)}\ . \tag{4}$$

These ratios are quite different from the ratios expected for a GDR in SCX, where the GDR is in a $T_z=T-1$ nucleus. For $T=2$, Eq. (4) gives the ratios 3:5:2, respectively. Therefore the GDR⊗IAS on ^{56}Fe should split into three components with the middle member about 50% stronger than the lower member. This is in close agreement with the observed ratios (Fig. 5). The intensity ratios obtained from the summed histogram (Fig. 2) are 3.1:5.0:3.4 from a Gaussian fit and 3.0:5.0:3.5 from a Lorentzian fit. Again there is a small enhancement of the upper isospin member relative to the above prediction.

A general treatment of isospin splitting in terms of isovector and isotensor potentials[34,35] gives the following relations for the energy splittings $\Delta E^+(T+1,T)$ and $\Delta E^-(T,T-1)$ for isovector excitations:

$$\Delta E^+=(T+1)[E_v+(2T-1)E_t]\ , \tag{5}$$

$$\Delta E^-=T[E_v-(2T+3)E_t]\ , \tag{6}$$

where E_v and E_t are the isovector and the isotensor energies. We can use our splitting energy to determine the isovector and the isotensor energies in Eqs. (5) and (6). If we use $\Delta E^+=3.5\pm1.0$ and $\Delta E^-=4.3\pm0.6$ MeV we obtain $E_v=1.46\pm0.43$ and $E_t=-0.098\pm0.044$ MeV. The deduced isovector and isotensor potentials from the present work are in agreement with the results from pion SCX data. For ^{60}Ni ($T=2$, same as our case), by comparing (π^+,π^0) and (π^-,π^0) data to the GDR, and setting arbitrarily $E_t=0$, a value of $E_v=0.88\pm0.67$ MeV was reported in the work of Erell *et al.*[24] The present values are consistent with the results from theoretical RPA calculations which give $E_v=1.06$ MeV and $E_t=-0.003$ MeV (Ref. 35) for ^{48}Ca. We note that these splittings for a collective dipole are only about one-half

those expected for single-particle excitations.[36] In fact Bohr and Mottelson estimate ΔE^+ to be about $V_1/2A(T_0+1)$ with $V_1 \simeq 130$ MeV in very good agreement with our results. They give no expression for ΔE^- but it is surprising that our ΔE^- is larger than our ΔE^+.

IV. SUMMARY

In conclusion, we have reported here the first observation of the isospin splitting of the giant dipole resonance built on the isobaric analog state [i.e., the analog of the GDR reached in (π^+,π^0) scattering] in pion double-charge-exchange scattering on ^{nat}Fe. The angular distributions for the three members have a dipole shape. Simple sequential-model calculations for a giant-dipole state built on the isobaric analog state give qualitatively, and surprisingly also quantitatively, a correct description of the measured cross sections and the angular-distribution shape. The observed cross-section ratio of the three members lower:middle:upper is in rough agreement with the values of 3:5:2 expected from simple isospin-coupling arguments. The energy splitting of the dipole IAS is somewhat larger than estimated for its analog GDR in single-charge-exchange scattering.

ACKNOWLEDGMENTS

We thank Helmut Baer, David Bowman, and Gerry Garvey for stimulating discussions. This work was supported in part by the United States Department of Energy, the Robert A. Welch Foundation, the National Science Foundation, and the United States–Israel Binational Science Foundation.

[1]D. M. Brink, doctoral thesis, University of Oxford, 1955; P. Axel, Phys. Rev. **126**, 671 (1962).
[2]G. F. Bertsch and R. A. Broglia, Physics Today **39** (No. 8), 44 (1986).
[3]J. O. Newton *et al.*, Phys. Rev. Lett. **46**, 1383 (1981).
[4]A. M. Sandorfi *et al.*, Phys. Lett. **130B**, 19 (1983).
[5]J. J. Gaardhøje *et al.*, Phys. Rev. Lett. **56**, 1783 (1986).
[6]C. A. Gossett *et al.*, Phys. Rev. Lett. **54**, 1486 (1985).
[7]M. A. Kovash *et al.*, Phys. Rev. Lett. **42**, 700 (1979).
[8]H. R. Weller *et al.*, Phys. Rev. C **25**, 2921 (1982).
[9]D. H. Dowell *et al.*, Phys. Rev. Lett. **50**, 1191 (1983).
[10]Kurt A. Snover, Annu. Rev. Nucl. Part. Sci. **36**, 545 (1986), and references therein; K. Snover, in *Proceedings of the Texas A&M Symposium on Hot Nuclei, College Station, Texas, 1987,* edited by S. Shlomo, R. P. Schmitt, and J. B. Natowitz (World Scientific, Teaneck, NJ, 1988), p. 72.
[11]Y. Alhassid, S. Levit, and J. Zingman, Phys. Rev. Lett. **57**, 539 (1986).
[12]A. Stolk *et al.*, Phys. Lett. B **200**, 13 (1988).
[13]D. B. Balamuth *et al.*, Phys. Rev. C **36**, 2235 (1987).
[14]J. D. Bowman *et al.*, Phys. Rev. Lett. **50**, 1159 (1983).
[15]H. W. Baer *et al.*, Phys. Rev. Lett. **49**, 1376 (1982).
[16]H. W. Baer *et al.*, Nucl. Phys. **A396**, 437c (1983).
[17]A. Erell *et al.*, Phys. Rev. Lett. **52**, 24 (1984).
[18]S. Mordechai *et al.*, Phys. Rev. Lett. **60**, 408 (1988); S. Mordechai *et al.*, in *Proceedings of the Texas A&M Symposium on Hot Nuclei, College Station, Texas, 1987,* edited by S. Shlomo, R. P. Schmitt, and J. B. Natowitz (World Scientific, Teaneck, NJ, 1988), p. 123.
[19]H. A. Thiessen *et al.*, Los Alamos Scientific Laboratory Report No. LA-6663-MS, 1977; S. J. Greene *et al.*, Phys. Lett. **88B**, 62 (1979).
[20]C. L. Morris *et al.*, Nucl. Instrum. Methods A **238**, 94 (1985).
[21]J. D. Bowman *et al.*, Phys. Rev. Lett. **46**, 1614 (1981).
[22]A. Gal, Phys. Rev. C **25**, 2680 (1982).
[23]N. Auerbach and A. Klein, Phys. Rev. C **28**, 2075 (1983).
[24]A. Erell *et al.*, Phys. Rev. C **34**, 1822 (1986).
[25]R. Leonardi, in *Pion-Nucleus Physics: Future Directions and New Facilities at LAMPF* (Los Alamos, NM, 1987), AIP Conf. Proc. No. 163, edited by R. J. Peterson and D. D. Strottman (AIP, New York, 1987), p. 321.
[26]E. Rost, computer code CHOPIN (unpublished). The code has been modified by one of us (C.L.M.) to calculate pion charge exchange reactions and renamed NEWCHOP.
[27]H. DeVries, C. W. DeJager, and C. DeVries, At. Data Nucl. Data Tables **36**, 495 (1987).
[28]W. B. Cottingame and D. B. Holtkamp, Phys. Rev. Lett. **45**, 1828 (1980).
[29]F. Irom *et al.*, Phys. Rev. C **34**, 2231 (1986).
[30]S. H. Rokni *et al.*, Phys. Lett. B **202**, 35 (1988).
[31]U. Sennhauser *et al.*, Phys. Rev. Lett. **51**, 1324 (1983).
[32]L. S. Kisslinger, Phys. Rev. **98**, 761 (1955).
[33]G. Rowe, M. Salomon, and R. H. Landau, Phys. Rev. C **18**, 584 (1978).
[34]R. Leonardi, Phys. Rev. C **14**, 385 (1976).
[35]N. Auerbach, A. Klein, and N. V. Giai, Phys. Lett. **106B**, 347 (1981).
[36]A. Bohr and B. Mottelson, *Nuclear Physics* (Benjamin, New York, 1975), Vol. II, p. 498.